Neurobiology of Pain 11 (2022) 100084

Contents lists available at ScienceDirect

Neurobiology of Pain

journal homepage: www.sciencedirect.com/journal/neurobiology-of-pain

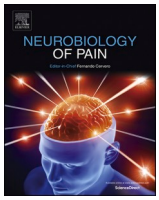

# Role of voltage-gated sodium channels in axonal signal propagation of trigeminal ganglion neurons after infraorbital nerve entrapment

Yatendra Mulpuri [a], Toru Yamamoto [a], Ichiro Nishimura [a,b], Igor Spigelman [a,*]

[a] Section of Oral Biology, School of Dentistry, University of California, Los Angeles, CA, USA
[b] Jane and Jerry Weintraub Center for Reconstructive Biotechnology, Division of Advanced Prosthodontics, School of Dentistry, University of California, Los Angeles, CA, USA

ARTICLE INFO

*Keywords:*
Trigeminal neuropathy
Infraorbital nerve entrapment
NaV1.3
NaV1.7
Nav1.8
Axonal mRNA transport
Axonal mRNA translation
Axonal signal propagation

ABSTRACT

Chronic pain arising from peripheral nerve injuries represents a significant clinical challenge because even the most efficacious anticonvulsant drug treatments are limited by their side effects profile. We investigated pain behavior, changes in axonal signal conduction and excitability of trigeminal neurons, and expression of voltage-gated sodium channels (NaVs) in the infraorbital nerve and trigeminal ganglion (TG) after infraorbital nerve entrapment (IoNE). Compared to Sham, IoNE rats had increased A- and C-fiber compound action potentials (CAPs) and Aδ component of A-CAP area from fibers innervating the vibrissal pad. After IoNE, A- and C-fiber CAPs were more sensitive to blockade by tetrodotoxin (TTX), and those fibers that were TTX-resistant were more sensitive to blockade by the NaV1.8 selective blocker, A-803467. Although NaV1.7 blocker, ICA-121431 alone, did not affect Aδ-fiber signal propagation, cumulative application with A-803467 and 4,9-anhydro-TTX significantly reduced the Aδ-fiber CAP in IoNE rats. In patch clamp recordings from small- and medium-sized TG neurons, IoNE resulted in reduced action potential (AP) depolarizing current threshold, hyperpolarized AP voltage threshold, increased AP duration, and a more depolarized membrane potential. While the transcripts of most NaVs were reduced in the ipsilateral TG after IoNE, NaV1.3, NaV1.7, and NaV1.8 mRNAs, and NaV1.8 protein, were significantly increased in the nerve. Altogether, our data suggest that axonal redistribution of NaV1.8, and to a lesser extent NaV1.3, and NaV1.7 contributes to enhanced nociceptive signal propagation in peripheral nerve after IoNE.

## Introduction

Peripheral branches of the trigeminal nerve provide sensory innervation to most craniofacial structures, and the cell bodies of their axons are housed in the Gasserian ganglion, which projects centrally into the brainstem trigeminal sensory nuclear complex. Compression or entrapment of trigeminal nerve branches from craniofacial trauma or iatrogenic procedures may result in chronic neuropathic orofacial pain (Benoliel et al., 2008). Although dissatisfactory due to side effects such as ataxia, fatigue, drowsiness, and memory impairment, membrane stabilizing drugs, including gabapentin and oxcarbazepine, have remained the first-line monotherapy for most peripheral neuropathy patients (Benoliel et al., 2012). Drugs that selectively modulate subtypes of voltage-gated ion channels, specifically those targeting voltage-gated sodium channels (NaVs) in nociceptors, may circumvent many of the undesirable effects associated with current medications, holding potential for efficacious treatment of neuropathic and other chronic pain disorders (Alsaloum et al., 2020; Waxman and Zamponi, 2014). NaVs regulate neuronal excitability and their activation is crucial for afferent signaling in nociceptors (Waxman et al., 1999). Numerous studies have reported the involvement of NaV1.3, NaV1.7, NaV1.8, and NaV1.9 in neuropathic pain pathophysiology, and clinical studies have shown abnormal expression of these NaV subtypes in peripheral axons or neuroma of trigeminal neuralgia and neuropathy patients (Bird et al., 2013; Siqueira et al., 2009).

The involvement of NaVs in neuropathic pain pathogenesis is mainly attributed to their increased expression and gain of function, and each NaV subtype is unique in its contribution (Lai et al., 2004). For example, NaV1.8 contributes to pain pathogenesis through its axonal redistribution in sensory neurons to the site of sciatic nerve constriction injury (Novakovic et al., 1998), and axonal depletion of NaV1.8 mRNA attenuates mechanical allodynia and thermal hyperalgesia after sciatic

* Corresponding author at: School of Dentistry, UCLA, 10833 Le Conte Avenue, 63-078 CHS Los Angeles, CA 90095-1668, USA.
*E-mail address:* igor@ucla.edu (I. Spigelman).

https://doi.org/10.1016/j.ynpai.2022.100084
Received 15 November 2021; Received in revised form 17 January 2022; Accepted 17 January 2022
Available online 21 January 2022

nerve entrapment (Ruangsri et al., 2011). Similarly, axonal depletion of NaV1.8 protein attenuates chronic pain symptoms after spinal nerve ligation injury (Gold et al., 2003). NaV1.3 channels, whose expression is normally highest during embryonic development, are significantly increased in somatosensory neurons after peripheral nerve injuries and contribute to increased neuronal excitability and mechanical allodynia (Samad et al., 2013; Waxman et al., 1994). In contrast, NaV1.7 gene-knockout studies have shown that its expression is essential in both somatosensory and sympathetic neurons for neuropathic pain development (Minett et al., 2012).

We previously showed that the increased peripheral nerve signal propagation and tetrodotoxin (TTX) resistance after sciatic nerve entrapment (SNE) in rats were related to the axonal redistribution of NaV1.8 mRNA and protein (Thakor et al., 2009). Although the neuronal mechanisms that underly the development of neuropathic pain are generally similar in somatic and orofacial regions, there are subtle yet significant differences between trigeminal and spinal nerves that affect responses to injuries and eventual development of neuropathic pain symptoms (DaSilva and DosSantos, 2012; Hargreaves, 2011; Sugimoto et al., 1986). For example, chronic constriction injury of infraorbital nerve (IoN) or inferior alveolar nerve (IaN) branches causes increased background activity and spontaneous afferent discharges in affected axons, which appear to persist longer in Aδ-fibers innervating the perioral region (Kitagawa et al., 2006; Robinson et al., 2004). Moreover, a recent study has shown that carbamazepine (CBZ) was more potent at inhibiting injury-induced neuropathic pain symptoms and increased axonal signal propagation of IoN than sciatic nerve, providing a possible explanation for the clinical effectiveness of CBZ in trigeminal neuralgia patients (Pineda-Farias et al., 2021). We hypothesized that these differences in electrophysiological properties of trigeminal and spinal nerves could be due to differential axonal accumulation of specific NaV subtypes likely via subcellular redistribution of their cognate mRNAs after peripheral nerve injuries. Here we used a rat model of trigeminal neuropathy induced by unilateral IoN entrapment to investigate the changes in axonal signal propagation and excitability of trigeminal ganglion neurons and the individual NaV subtypes contributing to these changes. Concomitantly, we examined changes in the expression of both mRNA and protein levels of individual NaV subtypes separately in peripheral nerve and trigeminal ganglion.

## Materials and methods:

### *Animals and drugs*

Adult male Sprague-Dawley rats (Envigo, Placentia, CA) weighing 300–325 g were used throughout the study. Rats were housed in the vivarium under a 12 h light–dark cycle (lights on at 6AM) with *ad libitum* access to food and water during the entire experiment. All experimental methods involving animal surgeries, behavioral testing, euthanasia, and tissue collection were carried out in accordance with the National Institute of Health guidelines for the care and use of laboratory animals and with approval from the Animal Research Committee of the University of California, Los Angeles. All drugs were obtained from Cayman Chemicals (Ann Arbor, MI). Stock TTX-citrate was dissolved in $dH_2O$, while A-803467, 4,9-anhydro-TTX, and ICA-121431 were dissolved in dimethyl sulfoxide (DMSO). For cumulative application of lipophilic drugs in nerve recordings, 5% DMSO in ACSF was used as vehicle.

### *Infraorbital nerve entrapment (IoNE)*

The IoNE model was adapted from the sciatic nerve entrapment model developed by Mosconi and Kruger (Mosconi and Kruger, 1996). Neuropathy was induced by placing two inert non-constrictive fixed diameter tygon cuffs around the infraorbital nerve (IoN). The surgical procedure to expose the IoN was as described previously (Kernisant et al., 2008). Briefly, in isoflurane-anesthetized rats, a rostro-caudal incision of ~7 mm long was made above left eye following the curvature of the frontal bone and the adherent muscle was gently teased from the bone to retract the orbital contents (Fig. 1A-B). The exposed IoN was separated from its surrounding connective tissue and slightly raised from the orbital floor with the aid of 4–0 nylon or chromic gut suture. Two sterile polyethylene (Tygon®, Fisher Scientific, Pittsburgh, PA) cuffs (OD: 2.4 mm, ID: 1.9 mm, 1.2–1.5 mm long) were placed around the IoN to induce entrapment injury. The incision above the eye was closed with 5–0 nylon suture. In Sham rats, the left IoN was exposed and separated from the surrounding connective tissue and the surgical incision was closed without placing cuffs. All animals were treated with a post-operative analgesic (carprofen 5 mg/kg, s.c., Zoetis Inc., Kalamazoo, MI) once daily for 2 days and an antibiotic (trimethoprim sulfamethoxazole 5 mL in 500 mL of drinking water, Pharmaceutical Associates Inc., Greenville, SC) for 7 days.

### *Mechanical allodynia testing*

A series of calibrated von Frey filaments (range: 1–30 g) were used to test for head withdrawal thresholds after vibrissal pad stimulation. Prior to actual testing, each animal was habituated in a Durham holder (Stoelting Co., Wood Dale, IL) for 5 min every day for 3 days. An average of 3 trials were performed on ipsilateral and contralateral vibrissal pads at baseline, 1-week, and 2-weeks post-surgery. Data were expressed as change from baseline.

### *Sample collection*

2–3 weeks following IoNE or Sham surgeries, rats were deeply anesthetized with isoflurane, decapitated, and the heads were quickly submerged in cold (0–4 °C) $Ca^{2+}$ free artificial cerebrospinal fluid (ACSF) containing (in mM): 125 NaCl, 2.5 KCl, 1.25 $NaH_2PO_4$, 2 $MgCl_2$, 26 $NaHCO_3$, 10 glucose, saturated with 95% $O_2$ and 5% $CO_2$. The heads were hemisected longitudinally and microdissected in cold $Ca^{2+}$ free ACSF to isolate ipsilateral IoN and trigeminal ganglion (TG). The IoN was incubated in regular ACSF (with 2 mM $CaCl_2$) for 1 h at room temperature before performing compound action potential (CAP) recordings and the TG was used for acute dissociation of TG neurons for patch clamp recordings. For quantitative measurements of mRNA and protein, the IoN and TG were placed immediately in RNAlater (Thermo Fisher Scientific, Carlsbad, CA) or −80 °C.

### *Compound action potential (CAP) recordings*

All CAP recordings were performed at room temperature (~24 °C) in an acrylic chamber continuously perfused with regular ACSF saturated with 95% $O_2$ and 5% $CO_2$. Borosilicate glass suction electrodes were used for recordings. The distal (peripheral) end of the nerve was inserted into a stimulating electrode and the proximal (central) end into a recording electrode. An artifact suppression electrode was placed next to the recording electrode. Signals from the recording and artifact suppression electrodes were fed into a differential amplifier (Dam 50, WPI, Sarasota, FL) in AC mode. A calibration pulse was included in the CAP recordings to estimate the resistance at the nerve/recording electrode junction. Signals from CAP recordings were further amplified (Brownlee Precision Instruments, Model 440, Santa Clara, CA), digitized at 10–20 kHz (Digidata 1440A, Molecular Devices, Union City, CA) and displayed on a computer screen using the pCLAMP 10 software (Molecular Devices). Nerve conduction was assessed by delivering square wave current pulses of fixed amplitude (0.2, 0.3, 0.5, 0.8, 1, 2, 3, 5, 8, and 10 mA, 0.1 ms duration for A-fiber CAP; 0.2, 0.3, 0.5, 1, 2, 3, 5, 8, 10, and 15 mA, 1 ms duration for C-fiber CAP), and the data for each stimulus strength were acquired by averaging 3 trials. Aβ-, Aδ-, and C-fiber CAPs were identified based on their conduction velocities (Djouhri and Lawson, 2004; Harper and Lawson, 1985; Villiere and McLachlan, 1996; Zotova and Arezzo, 2013), estimated by measuring the ratio of nerve

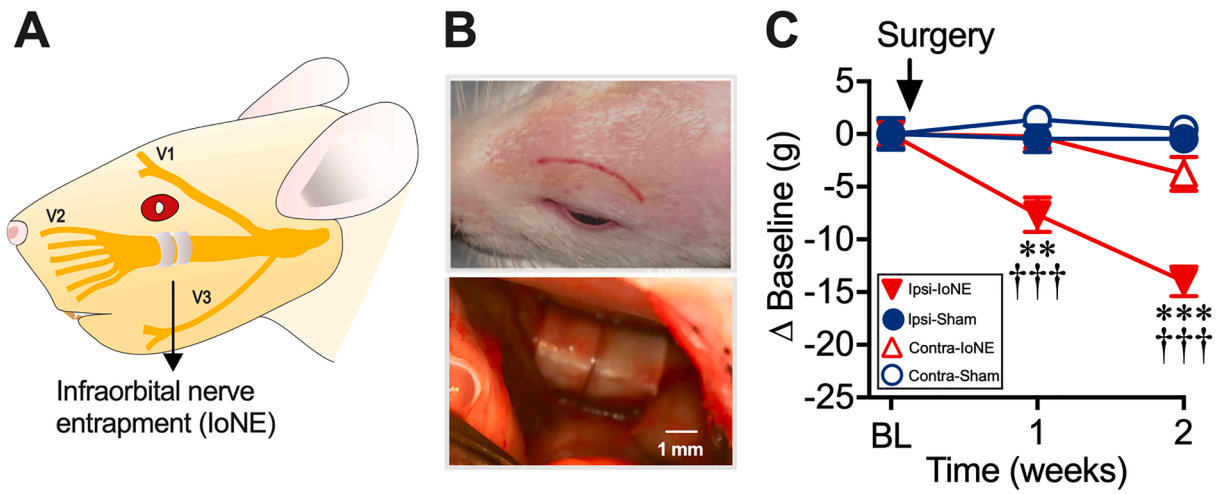


**Fig. 1.** Increased sensitivity to mechanical stimulation of vibrissal pad after infraorbital nerve entrapment (IoNE). A. Schematic illustration of a rat model of trigeminal neuropathy induced by placing 2 fixed-diameter non-constrictive tygon cuffs (OD: 2.4 mm; ID: 1.9 mm; Length: 1.2–1.5 mm) around the infraorbital nerve. B. The upper photographic image shows the site of surgical incision marked with red ink and the lower image shows 2 tygon cuffs placed around the infraorbital nerve lying on the orbital floor. The 1 mm scale bar in the lower image is shown to indicate the approximate size of tygon cuffs relative to the infraorbital canal. C. Time course of head withdrawal thresholds in response to von Frey stimulation expressed as change from baseline on the ipsilateral (ipsi) and contralateral (contra) sides of Sham and IoNE rats. **, $p < 0.01$; ***, $p < 0.001$ ipsi-Sham vs ipsi-IoNE; †††, $p < 0.001$ ipsi-IoNE vs contra-IoNE, two-way RM ANOVA (n = 8/group). (For interpretation of the references to colour in this figure legend, the reader is referred to the web version of this article.)

length (m) to conduction latency (s). The time it took for the signal to travel from the beginning of the stimulus artifact to the peak of CAP amplitude was determined as conduction latency. Recordings were monitored for CAP stabilization for 60–90 min before acquiring the stimulus-output response data and for 30–60 min after vehicle (5% DMSO) or drug application. CAP areas and amplitudes were normalized to the calibration pulse using pCLAMP 10 software. Investigators performing the IoN extractions and CAP recordings could not be blinded to the treatment of experimental animals.

*Acute dissociation of trigeminal ganglion (TG) neurons*

TG tissue corresponding to the maxillary division was microdissected in a cold (~4 ℃) modified Tyrode's solution containing (in mM): 130 NaCl, 20 $NaHCO_3$, 3 KCl, 4 $CaCl_2$, 1 $MgCl_2$, 10 HEPES, and 12 glucose with antibiotic/antimycotic solution (0.5%; Fisher Scientific, Hanover Park, IL). The minced tissues were incubated in collagenase (1 mg/ml, type I; Fisher Scientific) for 1 h at 37 °C, then in collagenase with trypsin/EDTA (0.2%; Fisher Scientific) for 1 h at 37 °C, followed by a 2 × wash with modified Tyrode's solution and gentle trituration with a fire-polished Pasteur glass pipette. Next, the cell suspension was mixed with bovine serum albumin (15%; Fisher Scientific) and centrifuged at 900 rpm for 10 min to remove myelin and debris. The pellet was resuspended with Neurobasal A (Fisher Scientific) containing B27 (2%), L-glutamine (0.2%), and antibiotic/antimycotic solution (0.1%), and cells were plated onto glass coverslips coated with poly-D-lysine/laminin (Fisher Scientific). The cells were incubated at 37 °C in a humidified 5% $CO_2$ chamber and used for recordings 1–6 h after plating.

*Patch clamp recordings and analysis*

The recording chamber (1 mL capacity) (Warner Instruments, Holliston, MA) was placed on the stage of an upright microscope (Olympus, Waltham, MA) and continuously perfused with an external solution at 2 mL/min using a peristaltic pump (Ismatec, Wertheim, Germany). All recordings were performed at room temperature (~24 °C). Healthy neurons were identified by their smooth and non-coarse cell surface. Neuron size was estimated by calculating the mean of the longest and shortest cross-sectional diameters with the aid of a calibrated eyepiece reticle under phase contrast illumination. Neurons were defined as small- (<30 μm), medium- (30–45 μm), and large- (>45 μm) diameter. In current clamp recordings, patch pipettes had resistance of 3–5 MΩ when filled with (in mM): 100 K-gluconate, 40 KCl, 0.3 $CaCl_2$, 1 EGTA, 10 HEPES, 2 Mg-ATP, 0.2 $Na_2GTP$; (pH 7.2 adjusted with KOH, 290 mOsm). Bath solution contained (in mM): 140 NaCl, 4 KCl, 2 $CaCl_2$, 2 $MgCl_2$, 10 HEPES, 10 glucose; (pH 7.4 adjusted with NaOH, 315 mOsm). Recordings began 3 min after establishing whole-cell configuration to ensure stable recording conditions. Electrophysiological signals were amplified (Multiclamp 700B, Molecular Devices), low-pass filtered at 1 kHz, and digitized at 10 kHz (Digidata 1440A, Molecular Devices). Data were acquired and analyzed off-line using pCLAMP 10 software (Molecular Devices). Cells were held at −70 mV for current-clamp measurements of intrinsic membrane parameters. Recordings were discarded if current injection >20 pA/pF was needed to keep the holding potential at −70 mV. Action potential (AP) amplitude was determined as the distance from the −70-mV holding potential to the peak. Threshold voltage was determined as the most depolarized membrane potential achieved without firing an AP. Only cells with AP amplitudes >70 mV were included in the analysis. Current threshold (pA) was the smallest amount of depolarizing current sufficient to evoke an action potential. All patch clamp recordings and analysis were performed by an investigator blinded to the treatment of the experimental animals. All solutions were made fresh daily.

*Quantitative PCR*

Total RNA was isolated from IoN and TG samples using PureLink RNA Mini Kit (Thermo Fisher Scientific). RNA (200 ng) was reverse transcribed with Advantage RT for PCR kit (Takara Bio USA, Inc., Mountain View, CA) and the relative mRNA levels of NaV subtypes were determined using a quantitative polymerase chain reaction method with the following TaqMan probes from Thermo Fisher Scientific: NaV1.1 (Rn00578439_m1), NaV1.3 (Rn01485332_m1), NaV1.5 (Rn00565502_m1), NaV1.6 (Rn00570506_m1), NaV1.7 (Rn00591020_m1), NaV1.8 (Rn00568393_m1), NaV1.9 (Rn00570487_m1), and GAPDH (Rn01775763_g1). The relative gene expression level was calculated with the $2^{-\Delta\Delta Ct}$ method, where GAPDH was used as an internal reference control.

*Quantitative protein analysis*

*Plasma membrane protein isolation*

Total cellular membrane fraction from frozen ipsilateral IoN and TG samples were isolated and samples were further processed to extract the plasma membrane fraction. Briefly, samples were lysed in an ice-cold homogenization buffer supplemented with protease inhibitor cocktail (Abcam, Cambridge, MA) using a tissue homogenizer (Tissue Ruptor II, Qiagen), centrifuged in 700*g* for 10 min at 4 °C, and the total membrane pellet was collected to extract plasma membrane fraction following manufacturer's protocol (Abcam). The extracted plasma membrane proteins were dissolved in 0.5% Triton X-100 in PBS, and the protein concentration was determined with a BCA protein assay (Thermo Fisher Scientific).

*Wes protein analysis*

For quantification of target proteins, we used the Wes system (ProteinSimple, San Jose, CA), an automated size-based separation and immunoassay platform for detection and characterization of protein molecular weights in denatured protein lysates. The Wes system automatically performs all the manual steps associated with traditional Western analysis and provides true quantification of results. Briefly, samples (0.5 mg/mL) were diluted in a Wes sample buffer, reduced, and denatured according to the manufacturer's protocol and run on a 66–440 kDa separation module (SM-W008, ProteinSimple). Primary antibodies for target proteins were diluted in Wes antibody diluent 2 as follows: NaV1.3 (1:20), NaV1.6 (1:20), NaV1.7 (1: 150), NaV1.8 (1:100), and NaV1.9 (1:20) (Alomone Labs, Jerusalem, Israel). Wes anti-rabbit detection module (DM-001, ProteinSimple) was used for chemiluminescent detection. Spectral peaks were quantified on Compass for Simple Western software. All NaV antibodies used in this study recognized two spectral peaks at 165 kDa and 265 kDa, similar to those shown in the manufacturer's Western blot results. However, only the 265 kDa peaks, which correspond to the predicted size of NaV proteins, were included in the quantitative analysis (Baroni et al., 2014; Salvatierra et al., 2018; Sun et al., 2018). All target proteins were normalized to total protein for quantification. Specificity of each antibody was verified by comparing spectral peaks with or without pre-adsorption with a control antigen at 2 × Ab concentration.

*Data analysis*

Data were expressed as mean ± standard error of mean (S.E.M). Two group comparisons were made with unpaired *t*-test. Analysis of variance (ANOVA) with Sidak's multiple group comparison test was used for post-hoc comparisons. The F-statistic values of ANOVA are reported in Table 1. $P < 0.05$ was considered statistically significant. All statistical analyses were performed using Prism 7 software (GraphPad Software Inc., La Jolla, CA).

## Results

*Mechanical allodynia, increased infraorbital nerve signal propagation, and enhanced sensitivity to TTX and NaV1.8 blocker after IoNE*

Approximately two weeks after Sham or IoNE surgery (Fig. 1A, B), significant mechanical allodynia was observed in the IoNE group in response to von Frey stimulation of ipsilateral but not contralateral vibrissal pads (Fig. 1C). Subsequently, rats were euthanized, and *ex vivo* ipsilateral IoNs were prepared for CAP recordings (Fig. 2A-C). A-fiber CAP areas and C-fiber CAP amplitudes were significantly increased in the IoNE group compared to Sham group (Fig. 2D, E). To determine NaV contribution to the changes in axonal signal propagation after IoNE, the non-selective NaV blocker, TTX (100 nM and 300 nM) and NaV1.8 specific blocker, A-803467 (5 μM) were applied consecutively and the percent of pre-drug A-CAP area and C-CAP amplitude remaining after 35 min of each application estimated (Fig. 3A, B). The decrease in A- and C-fiber CAPs after applying TTX (100 nM) was not significantly different between IoNE and sham groups (Fig. 3C, D). However, the decrease in A-fiber CAP area (Sham: 45.4 ± 9.8%; IoNE: 8.9 ± 3.2%; $p < 0.01$) and C-fiber CAP amplitude (Sham: 71.5 ± 9.8%; IoNE: 42.8 ± 5.2%; $p < 0.05$) after TTX (300 nM) was significantly greater from IoNE compared to Sham rats, implying greater TTX sensitivity of axonal conduction block after IoNE. In addition, applying TTX (300 nM) with the NaV1.8 specific blocker, A-803467 (5 μM) further reduced A-fiber (Sham: 34.3 ± 8.4%; IoNE: 1.2 ± 0.4%; $p < 0.05$) and C-fiber (Sham: 66.3 ± 8.9%; IoNE: 31.3 ± 5.1%; $p < 0.01$) CAPs, with greater decreases in the IoNE group compared to Sham. This result suggested that IoNE induced increases in NaV1.8 expression or function in a subset of axons resistant to axonal conduction block by TTX.

**Table 1**
F-statistic values of mean differences obtained from two-way ANOVA comparisons.

| Figure | Column Factor | Row Factor | Interaction |
|---|---|---|---|
| Fig. 1C | Group F (3, 28) = 13.77; $p < 0.001$ | Time F (2, 56) = 16.05; $p < 0.001$ | Group × Time F (6, 56) = 9.01; $p < 0.001$ |
| Fig. 2D | Group F (1, 270) = 7.175; $p < 0.01$ | Stimulus F (9, 270) = 34.12; $p < 0.001$ | Group × Stimulus F (9, 270) = 0.56; $p>0.05$ |
| Fig. 2E | Group F (1, 110) = 18.51; $p < 0.001$ | Stimulus F (9, 110) = 47.88; $p < 0.001$ | Group × Stimulus F (9, 110) = 1.84; $p>0.05$ |
| Fig. 3C | Group F (1, 36) = 17.68; $p < 0.001$ | Treatment F (2, 36) = 25.67; $p < 0.001$ | Group × Treatment F (2, 36) = 2.07; $p>0.05$ |
| Fig. 3D | Group F (1, 39) = 16.2; $p < 0.001$ | Treatment F (2, 39) = 7.11; $p < 0.01$ | Group × Treatment F (2, 39) = 2.26; $p>0.05$ |
| Fig. 4C | Group F (1, 14) = 1.07; $p>0.05$ | Stimulus F (9, 126) = 30.02; $p < 0.001$ | Group × Stimulus F (9, 126) = –0.91; $p>0.05$ |
| Fig. 4D | Group F (1, 140) = 5.88; $p < 0.05$ | Stimulus F (9, 140) = 29.11; $p < 0.001$ | Group × Stimulus F (9, 140) = 1.83; $p>0.05$ |
| Fig. 4E | Group F (1, 49) = 1.8; $p>0.05$ | Treatment F (3, 49) = 95.45; $p < 0.001$ | Group × Treatment F (3, 49) = 1.47; $p>0.05$ |
| Fig. 4F | Group F (1, 49) = 39.05; $p < 0.001$ | Treatment F (3, 49) = 40.11; $p < 0.001$ | Group × Treatment F (3, 49) = 4.12; $p>0.05$ |
| Fig. 6A | Group F (1, 97) = 85.89; $p < 0.001$ | mRNA F (6, 97) = 11.81; $p < 0.001$ | Group × mRNA F (6, 97) = 11.81; $p < 0.001$ |
| Fig. 6B | Group F (1, 98) = 38.32; $p < 0.001$ | mRNA F (6, 98) = 3.81; $p < 0.01$ | Group × mRNA F (6, 98) = 3.81; $p < 0.01$ |

*Changes in axonal signal conduction of vibrissal pad afferents after IoNE*

Allodynia is a prominent symptom of trigeminal neuropathies (Shinoda et al., 2021), and IoNE but not sham surgery induced significant mechanical allodynia in the ipsilateral vibrissal pad region (Fig. 1C). To investigate if the mechanical allodynia caused by IoNE is related to changes in the axonal conduction of affected axons, we recorded CAPs from the IoN fiber bundles selectively innervating the vibrissal pad (Fig. 4A). Recordings revealed prominent Aβ- and Aδ-fiber CAPs (Fig. 4B), but only a very small C-CAP that could not be resolved in most of these recordings (not shown). IoNE had no significant effect on Aβ-fiber CAP area (Fig. 4C). By contrast, the Aδ-CAP area was significantly increased at higher stimulus strengths in the IoNE group compared to Sham (Fig. 4D).

*Role of NaV subtypes in axonal signal conduction of vibrissal pad afferents after IoNE*

Next, we investigated the role of NaV subtypes contributing to the increased signal propagation of Aδ-fibers through the cumulative application of subtype-specific NaV blockers and determining the percent of pre-drug CAP remaining 35 min after each application (Fig. 4E-F). The concentrations of selective blockers were chosen based on published efficacy and selectivity studies (Klein et al., 2017; McCormack et al., 2013; Rosker et al., 2007; Vysokov et al., 2019; Xie et al., 2019). Since the sensitivity of IoN to axonal conduction block by TTX was significantly increased after IoNE, and the TTX-sensitive

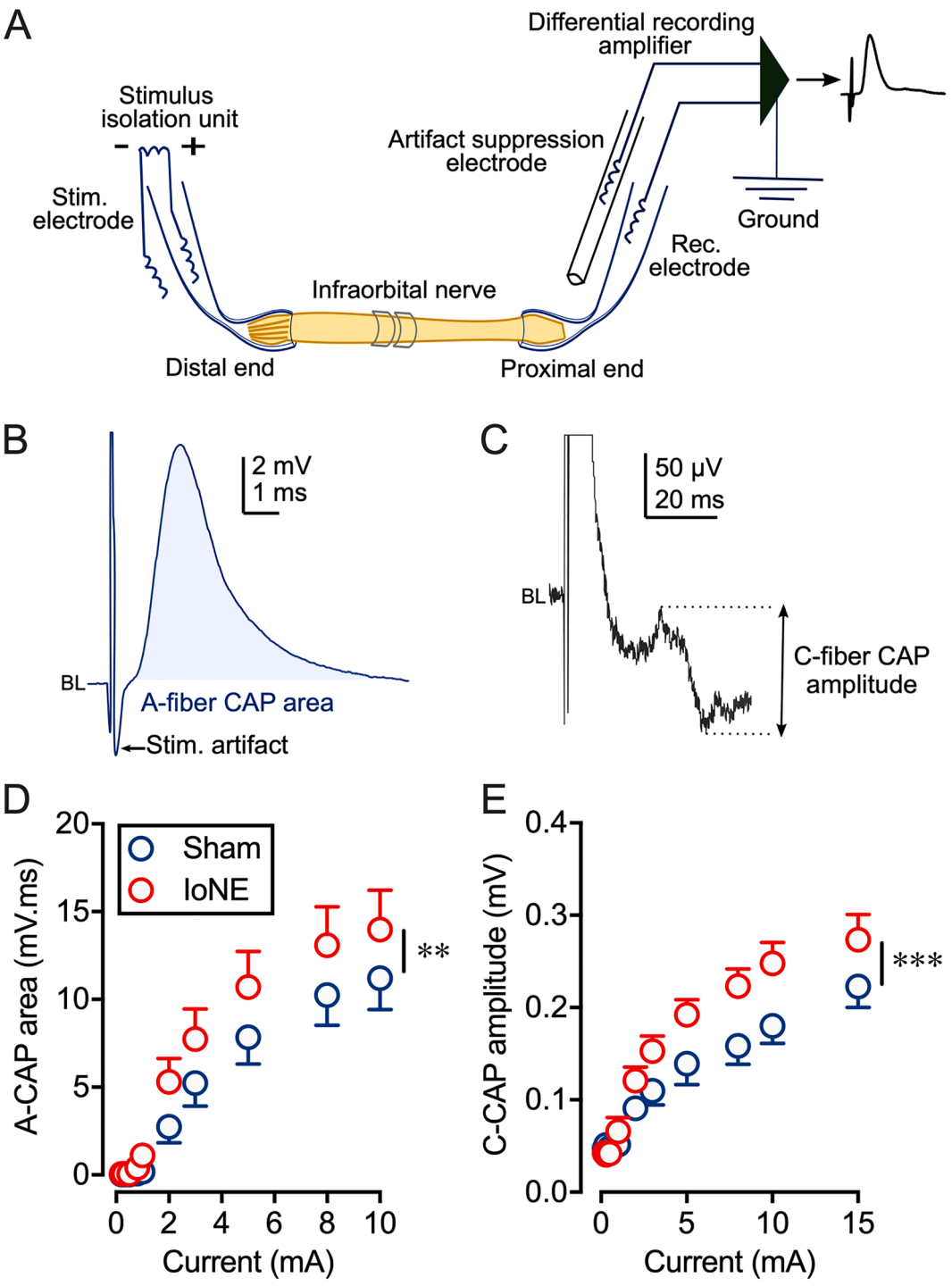


**Fig. 2.** Infraorbital nerve entrapment (IoNE) increases A- and C-fiber axonal signal propagation measured at 2–3 weeks post-surgery. A. Schematic illustration of recording arrangement. The distal end of the nerve was placed into a stimulating suction electrode and the evoked compound action potentials (CAPs) were recorded from the proximal end of the nerve with a recording suction electrode. Signals from the artifact suppression and recording electrodes were fed into a differential recording amplifier, digitized, and stored for off-line analysis. B-C: Sample recording traces show A-fiber CAP area (B) and C-fiber CAP amplitude (C) along with stimulus artifacts. D. Stimulus-output plot of A-fiber CAP area for infraorbital nerves ipsilateral to IoNE (n = 15) and Sham (n = 14) surgery rats. E. Stimulus-output plot of C-fiber CAP amplitude of infraorbital nerves ipsilateral to IoNE (n = 7) and Sham (n = 6) surgery rats. **, $p < 0.01$; ***, $p < 0.001$ IoNE vs Sham; two-way ANOVA.

NaV1.7 channel has a crucial role in nociception (Chew et al., 2019; Hoffmann et al., 2018), we first applied a NaV1.7 specific blocker, ICA-121431 (1 µM). In both groups, there were no significant changes in the Aβ- or Aδ-CAP area after normalizing to the vehicle control. The cumulative application of a NaV1.8 specific blocker, A-803467 (5 µM) with the NaV1.7 blocker, significantly reduced the Aδ-fiber CAP area in the IoNE group (Sham: 100.9 ± 4.6%; IoNE: 84.6 ± 2%; $p < 0.05$). Moreover, the cumulative application of NaV1.7 and NaV1.8 blockers and 4,9-anhydro-TTX (0.5 µM) further reduced the Aδ-fiber CAP area in the IoNE group compared to Sham (Sham: 87.2 ± 4.7%; IoNE: 69.2 ± 2.2%; $p < 0.01$). This increased sensitivity of Aδ-fiber CAP in the IoNE group was also observed after applying the NaV1.8 blocker with TTX (100 nM)

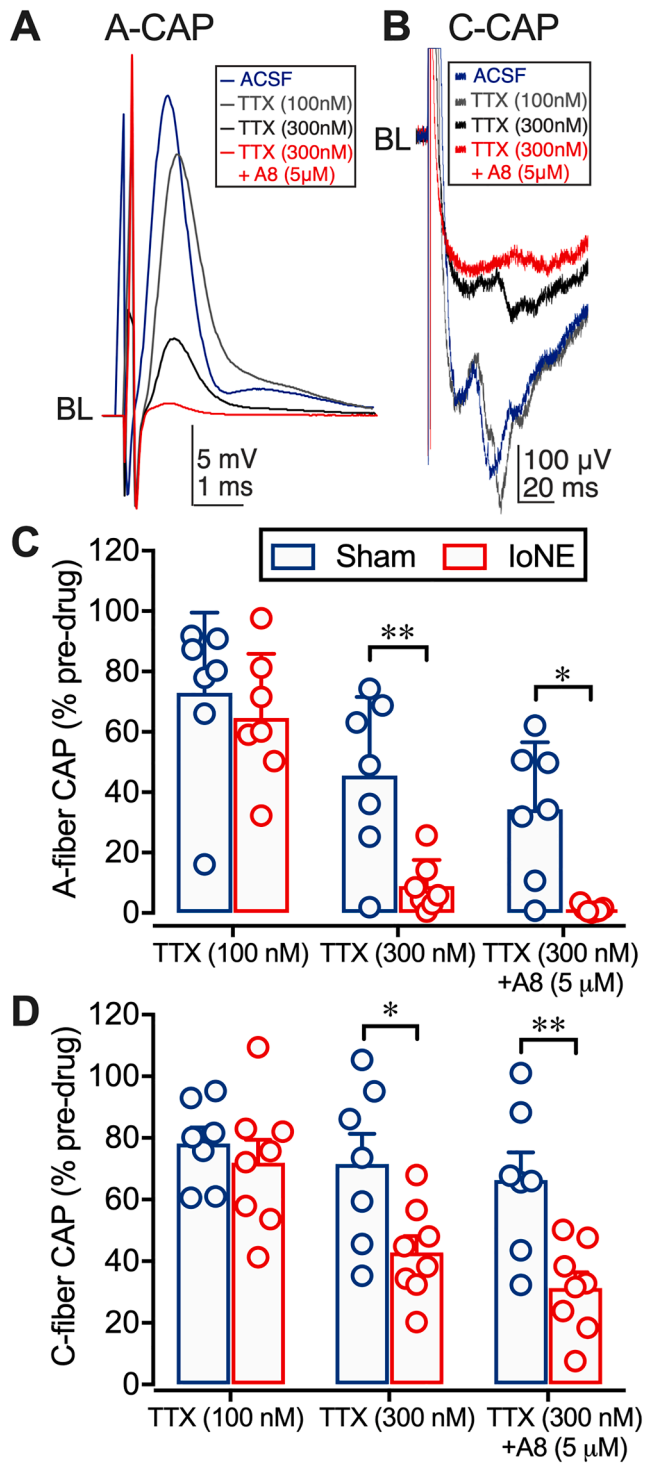


**Fig. 3.** Increased sensitivity of infraorbital nerve to axonal conduction block by tetrodotoxin (TTX) and NaV1.8 blocker after IoNE. A-B: Sample recording traces from an IoNE rat show decreases in A-fiber CAP (10 mA; 0.1 ms) area and C-fiber CAP (15 mA; 1 ms) amplitudes after TTX and NaV1.8 blocker, A-803467 (A8). C-D: Decreases in A-fiber CAP area and C-fiber CAP amplitude are significantly greater in IoNE compared to Sham after bath application of TTX (300 nM) and TTX (300 nM) + A-803467 (5 μM). However, the decrease in A- and C-fiber CAP measurements of IoNE group are not significantly different from Sham after TTX (100 nM). *, $p < 0.05$; **, $p < 0.01$ Sham vs IoNE; two-way ANOVA, Sidak's multiple comparison test (n = 7–8/group).

(Sham: 74.1 ± 8.6%; IoNE: 39.4 ± 5%; $p < 0.001$). These findings suggest that increased activation of NaV1.8 contributes to axonal signal conduction after IoNE, at least in the stimulated Aδ fibers innervating the vibrissal pad. The increased sensitivity of the Aδ-fiber CAP area to 4,9-anhydro-TTX and TTX implies that other TTX-sensitive channels, including NaV1.3, may contribute to the enhanced axonal signal propagation of these afferents after IoNE.

*Increased excitability of dissociated TG neurons after IoNE*

Current clamp recordings revealed significant differences in the membrane properties of small-medium diameter TG neurons between Sham and IoNE groups. The average size of TG neurons from Sham and IoNE rats in current-clamp recordings was 26.9 ± 2.3 μm (small-diameter: 8 neurons, medium-diameter: 6 neurons) and 27.1 ± 2.0 μm (small-diameter: 13 neurons, medium-diameter: 3 neurons), respectively. Action potential (AP) waveforms generated in TG neurons of Sham and IoNE rats by square-pulse stimulation are shown in Fig. 5A. The threshold current intensities for evoking APs were significantly decreased in the IoNE vs Sham group (Fig. 5B). In the absence of differences in AP amplitude (Fig. 5C), the AP duration was significantly increased in the IoNE group (Fig. 5D), and the voltage threshold for first AP was significantly more hyperpolarized in the IoNE group (Fig. 5E). The resting membrane potential was significantly more depolarized in the IoNE group compared to Sham group (Fig. 5F).

*Changes in NaV mRNA levels in IoN and TG after IoNE*

In our previous RNA-Seq study we observed changes in axonal localization of several hundred mRNAs induced by sciatic nerve entrapment (Hirai et al., 2017). To determine the effect of IoNE on the levels and relative localization of various NaV subtype mRNAs, we measured their steady-state levels separately in ipsilateral TG and IoN of Sham and IoNE rats at two weeks post-surgery. Two-way ANOVA revealed a significant increase in the expression of NaV1.3, NaV1.7, and NaV1.8 mRNAs in the IoN of IoNE group compared to Sham group (Fig. 6A). By contrast, in the TG of IoNE rats, NaV1.1, NaV1.5, NaV1.6, NaV1.8, and NaV1.9 mRNAs were significantly decreased compared to Sham rats (Fig. 6B). These data suggested relative redistribution of select NaV subtype mRNAs from the TG somata to their peripheral axons after IoNE.

*Changes in NaV protein levels in IoN and TG after IoNE*

In order to better relate the contribution of different NaV subtypes to IoNE-induced changes in signal propagation of peripheral axons and excitability of TG neuronal somata, we quantified the NaV subtype proteins in the plasma membrane fractions of ipsilateral IoN and TG from Sham and IoNE rats. Analysis revealed a significant increase in the membrane expression only of NaV1.8 protein in the IoN of IoNE group vs Sham group (Fig. 7A-E). In the TG, only the plasma membrane expression of NaV1.7 protein was significantly decreased in the IoNE group vs Sham group (Fig. 7F-J). These data confirmed the increased contribution of NaV1.8 to the signal propagation of IoN fibers after IoNE.

## Discussion

Anticonvulsants targeting NaVs have been used clinically to treat trigeminal neuralgia and other orofacial neuropathies for more than three decades. However, the role of individual NaV subtypes in the electrophysiological changes of primary afferents after trigeminal nerve injuries remains to be investigated. The current study investigated IoNE-induced alterations in excitability of trigeminal ganglion neurons and the role of NaVs in axonal signal propagation. Our results show significantly increased signal propagation in A- and C-fibers after IoNE compared to Sham, with enhanced sensitivity to axonal conduction

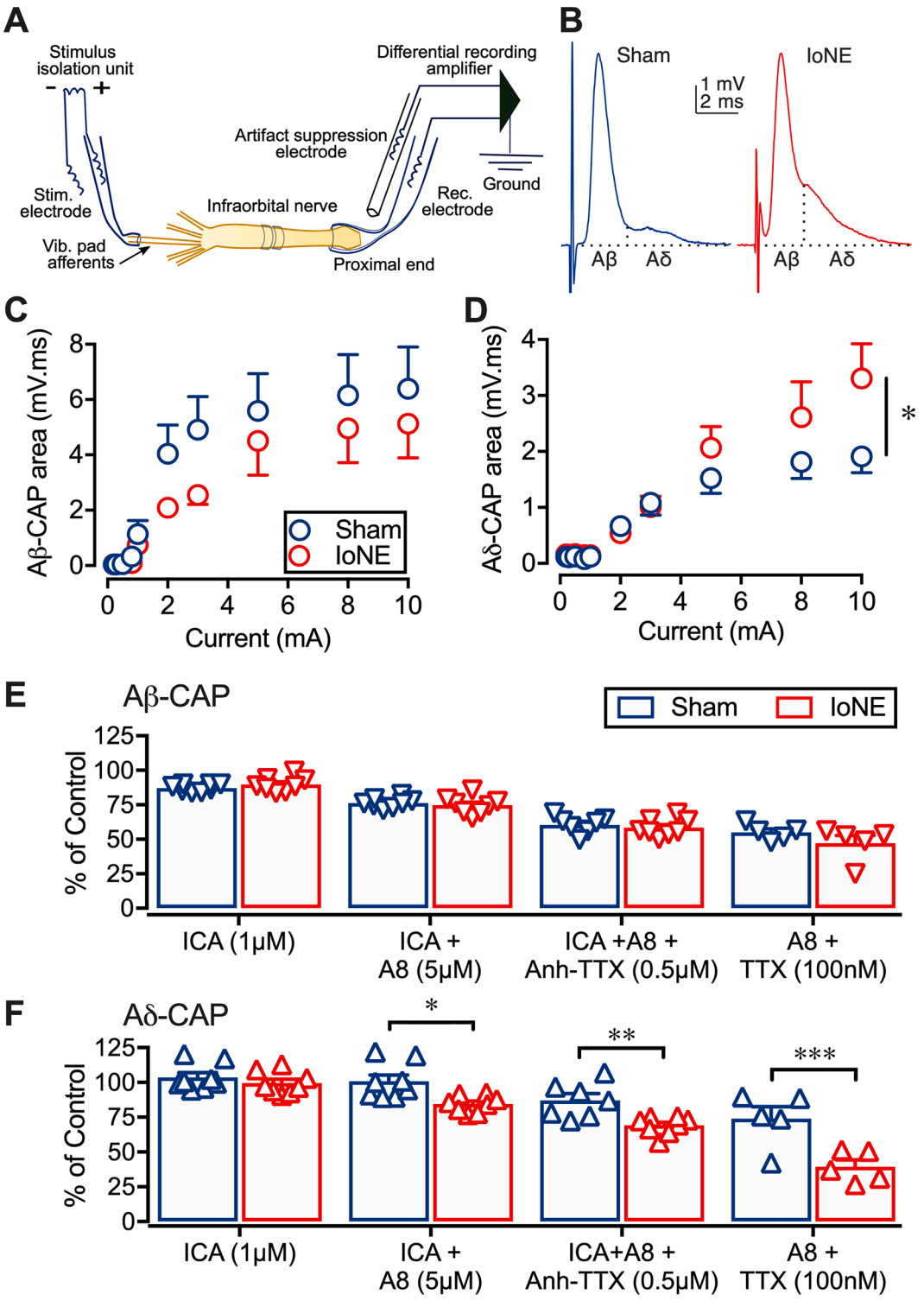


**Fig. 4.** Infraorbital nerve entrapment (IoNE) selectively increases the axonal signal propagation of Aδ-fibers innervating the vibrissal pad. A. Schematic of recording arrangement showing the peripheral end of vibrissal pad afferents placed into a stimulating suction electrode and the compound action potentials (CAP) recorded from the proximal end of the nerve with a recording suction electrode. The signals from the artifact suppression and recording electrodes were fed into a differential recording amplifier, digitized, and stored for off-line analysis. B. Sample recording traces show CAP areas (indicated by dotted lines) of Aβ- and Aδ-fibers of IoNE and Sham nerves acquired at 10 mA stimulus strength, 0.1 ms duration. The vertical dotted lines indicate an approximate conduction velocity of 8.5 m/s, used to segregate Aβ- and Aδ-fiber CAP areas C-D: Stimulus-output response plots show no significant difference in CAP areas of Aβ-fibers between IoNE and Sham nerves. In contrast, IoNE significantly increased the Aδ-fiber CAP area of infraorbital nerve samples at higher stimulus strengths compared to Sham nerves. E-F: Changes in Aβ- and Aδ-fiber CAP areas expressed as percent of vehicle control (DMSO) after cumulative application of NaV1.7 blocker (ICA-121431, 1 μM), NaV1.8 blocker (A-803479, 5 μM), 4,9-anhydro-TTX (0.5 μM), and TTX (100 nM). *, $p < 0.05$; **, $p < 0.01$; ***, $p < 0.001$ Sham vs IoNE; two-way ANOVA, Sidak's multiple comparison test (n = 5–8/group).

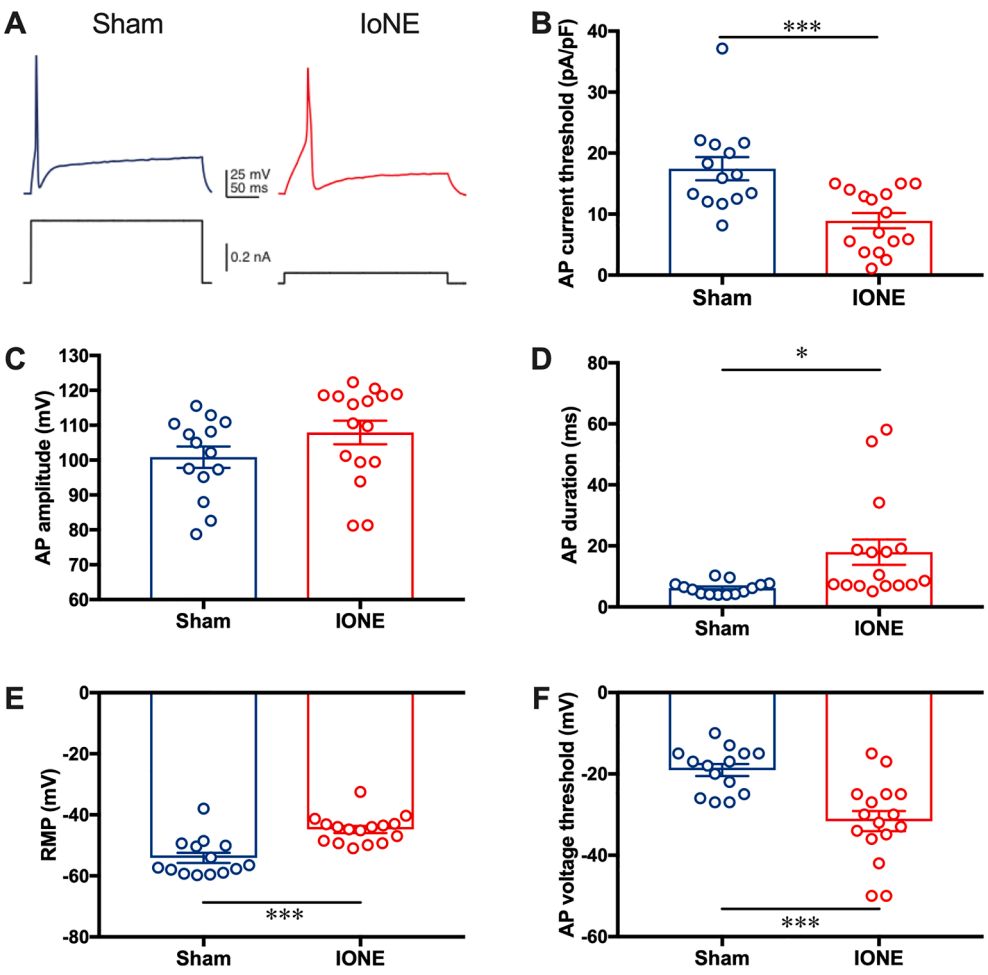


**Fig. 5.** Membrane properties of trigeminal ganglion (TG) neurons from Sham and IoNE groups. A. Sample traces of action potential (AP) waveforms in response to depolarizing square wave currents from TG neurons of Sham and IoNE rats collected at 2 weeks post-surgery. B. Threshold intensities for evoking APs. C. AP amplitude. D. AP duration measured at half-amplitude. E. Resting membrane potential (RMP). F. The voltage threshold for first AP. **, $p < 0.01$; ***, $p < 0.001$, Sham (n = 14 neurons/6 rats) vs IoNE (n = 16 neurons/7 rats), unpaired *t*-test.

block by 300 nM TTX, as well as increased sensitivity of the TTX-resistant component to the NaV1.8 selective blocker. While an increase in TTX permeability might have contributed to its enhanced sensitivity after IoNE, due to the disruption of tight junctions and blood-nerve barrier from nerve injury (Reinhold et al., 2018), the lack of such effects in the SNE neuropathy model (Thakor et al., 2009) suggests that these changes are specific to the IoN. The increased CAP size and its sensitivity to TTX after IoNE could be due to increased contributions from the various TTX-sensitive NaV subtypes. We found a trend to increases in all TTX-sensitive NaV mRNAs, but significant upregulation of only NaV1.3 and NaV1.7 axonal mRNAs, supporting their role in increased CAPs and TTX sensitivity after IoNE. Contrary to our mRNA findings, we did not observe a significant change in any of the TTX-sensitive NaV membrane protein levels. However, a previous study has shown increased axonal expression of NaV1.3 protein after the IoN injury (Liu et al., 2020). This discrepancy in observations on NaV1.3 expression might have resulted from measuring the total vs. plasma membrane protein levels. Although we did not measure NaV1.1 protein levels in this study, a previous study has shown its axonal upregulation after IoN injury, which correlates with its significant role in axonal conduction after the IoN injury (Pineda-Farias et al., 2021). We suspect that similar increased contributions of NaV1.1 and NaV1.3 channels to action potential propagation could mediate the increased TTX sensitivity after IoNE.

The enhanced sensitivity of the TTX-resistant component of CAP to blockade by the selective NaV1.8 inhibitor after IoNE is consistent with the increased TTX resistance of the sciatic nerve seen in spinal nerve (Gold et al., 2003) and sciatic nerve (Thakor et al., 2009) injury models, both of which exhibited increased axonal levels of NaV1.8 mRNA or protein. In these studies, antisense- or shRNA-mediated selective depletion of axonal NaV1.8 could be directly related to the suppression of injury-induced pain behaviors (Gold et al., 2003; Ruangsri et al., 2011). In the current study, increased sensitivity to the selective NaV1.8 inhibitor after IoNE could also be related to the increases in IoN steady-state levels of both NaV1.8 mRNA and protein. Thus, increased contribution of NaV1.8 signaling appears common to trigeminal and spinal nerve injuries.

After IoNE, we observed significant increases in the Aδ but not Aβ component of A-fiber CAP during selective activation of vibrissal pad afferents. These findings resemble the reported persistent increases in the Aδ-fiber vibrissal pad afferent excitability after the IoN injury (Kitagawa et al., 2006). Interestingly, the NaV1.7 specific inhibitor alone did not affect the Aδ-fiber signal conduction, whereas cumulative application of NaV1.7, NaV1.6, and NaV1.8 specific inhibitors and TTX, reduced the Aδ-fiber CAP area to a significantly greater extent in the IoNE compared to Sham group. The main implication of these findings is that functional NaV1.3 and NaV1.8 channels participate in the IoNE-induced increases in axonal signal conduction in Aδ afferents innervating the vibrissal pad. Although both NaV1.7 and NaV1.8 channels are expressed in spinal A and C nociceptors (Black et al., 2012; Daou et al., 2016), the lack of effect of NaV1.7 blocker on the Aδ CAP of vibrissal pad afferents suggests that these fibers may not depend on functional NaV1.7 channels for axonal conduction. It was shown in a recent study that NaV1.7 is essential for axonal propagation between cutaneous terminals and DRG neurons in only around two-thirds of nociceptive neurons (Goodwin et al., 2021). Suppressing the activity of NaV1.8-expressing neurons suppresses cutaneous allodynia after neuropathic injury (Daou et al., 2016), and NaV1.8 expression is also essential for ongoing

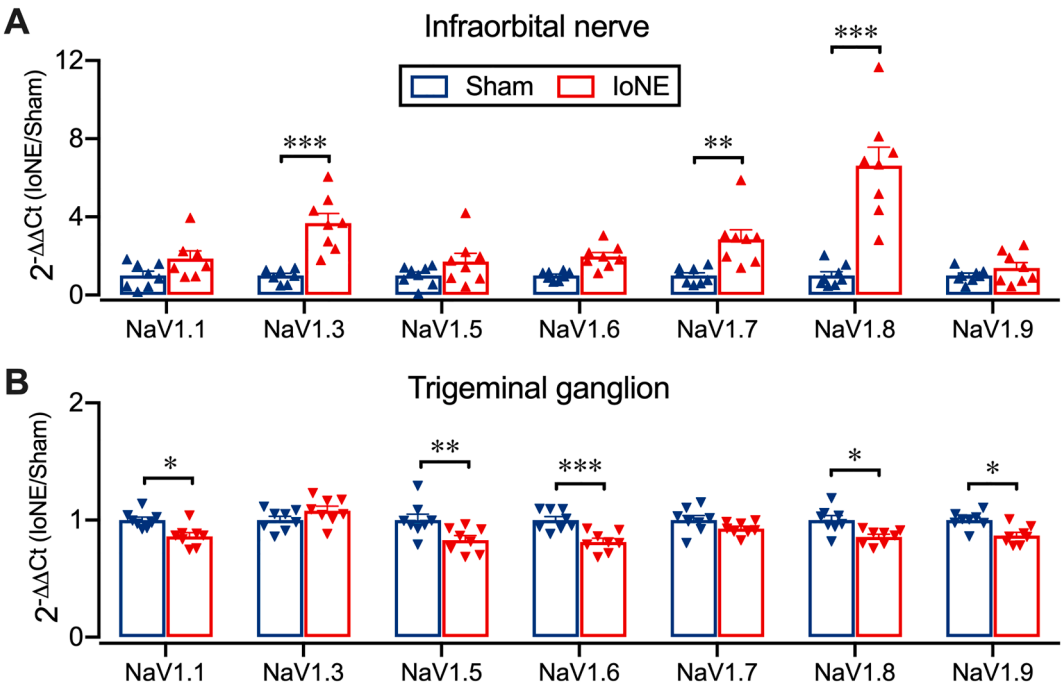


**Fig. 6.** Changes in the expression of voltage gated sodium channel (NaV) mRNAs in the ipsilateral infraorbital nerves and trigeminal ganglia of Sham and infraorbital nerve entrapment (IoNE) rats measured at 2 weeks post-surgery. A. IoNE selectively increased NaV1.3, NaV1.7, and NaV1.8 mRNAs in the infraorbital nerve, expressed as fold change vs. sham. B. However, in the trigeminal ganglion, IoNE significantly reduced the mRNA levels of NaV1.1, NaV1.5, NaV1.6, NaV1.8, and NaV1.9. Expression of all NaV mRNAs were normalized to the loading control, GAPDH mRNA and to the mean of Sham group. *, $p < 0.05$; **, $p < 0.01$; ***, $p < 0.001$ Sham vs IoNE, two-way ANOVA (n = 8 rats/group).

or spontaneous activity in injured C- and A-fiber neurons, including the fast-conducting Aδ-fibers (Roza et al., 2003). The current findings resemble those reported in a previous study where the addition of NaV1.8 inhibitor, A-803467 silenced the subset of skin afferents not silenced by NaV1.7 blockade alone in mouse thoracic skin-nerve preparations (Jurcakova et al., 2018). Although A-803467 could not translate to the clinic due to poor oral bioavailability, dexpramipexole, an inhibitor of eosinophilic inflammation with good oral bioavailability and clinical safety profile, was shown to selectively inhibit NaV1.8 channels and provide analgesia in sciatic nerve injury, chemotherapy-induced peripheral neuropathy, and diabetic peripheral neuropathy models (Bozik et al., 2011; Urru et al., 2020).

We could not investigate the changes in signal conduction of vibrissal pad C-fiber afferents because of the small C-CAP amplitude, which could not be resolved in most recordings. The relative proportion of myelinated and unmyelinated fibers in the stimulated nerve influences the size and shape of A- and C-fiber CAPs (Gasser and Grundfest, 1939), and previous studies have identified significant differences in the histological composition of trigeminal vs. spinal nerves. Though many studies showed that spinal nerves contain higher proportion of unmyelinated C-fibers (low A/C-fiber ratio) (Alpsan and Lal, 1980; Smith et al., 2012), trigeminal branches innervating the perioral region are predominantly composed of medium-large diameter myelinated afferents (high A/C-fiber ratio) (Sugimoto et al., 1986; Sugimoto et al., 1988). We suspect that the very small C-fiber CAP amplitudes observed in current IoN recordings could be due to low abundance of C-fibers in the stimulated vibrissal pad afferents. Overall evidence suggests that these subtle variations in the composition and spatial organization of primary afferent fibers in the injured trigeminal branches influence pain quality, location, and temporal features of trigeminal neuropathies (DaSilva and Dos-Santos, 2012). Moreover, the phenotypic characteristics of abnormal Aδ-fiber signaling such as paroxysmal attacks of electric shock-like pain observed in many trigeminal neuralgia patients suggest that Aδ-fibers play a crucial role in the pathophysiology of trigeminal neuropathic pain disorders (Koh et al., 2021).

It was shown in a previous study that 4,9-anhydro-TTX blocks mouse NaV1.6 currents with an $IC_{50}$ of 7.8 nM (Rosker et al., 2007). Although its specificity for rat NaV1.6 has not been extensively investigated, their findings found that 4,9-anhydro-TTX inhibits rat NaV1.3 with an $IC_{50}$ of 341 nM. In our IoN recordings, application of 4,9-anhydro-TTX at 10–300 nM showed no significant effect on A-fiber CAP area (Supp. Fig. 1). However, the further reduction of Aδ-fiber CAP area in the IoNE group after the cumulative application of 4,9-anhydro-TTX (0.5 μM) with NaV1.7 and NaV1.8 blockers could have resulted from the inhibition of NaV1.3 channels to some extent. The involvement of NaV1.3 is also supported by findings from our molecular studies showing axonal upregulation of NaV1.3 mRNA after IoNE. The current findings are also in agreement with a previous study showing a significant reduction of Na currents after the cumulative application of 4,9-anhydro-TTX (0.5 μM) with NaV1.7 and NaV1.8 blockers in cultured DRG neurons subjected to distal axotomy in vitro (Vysokov et al., 2019). Similar species differences in NaV selectivity have also been reported for ICA-121431, a selective blocker of human and mouse NaV1.1 and NaV1.3 channels ($IC_{50}$ = 19 nM), which also exhibits potent inhibition of rat NaV1.7 (McCormack et al., 2013).

IoNE significantly increased the excitability of small-medium sized TG neurons, as observed by their reduced current threshold for evoking APs, hyperpolarized AP voltage threshold, increased AP duration, and a more depolarized RMP. The changes in AP thresholds could be due to alterations in the function of somatic NaV subtypes. However, changes in AP duration and RMP suggest alterations of $K^+$ channels which are known to influence the RMP and AP repolarization. These include members of the KCNK family leakage $K^+$ channels which contribute to the RMP and the A-type Kv4.3 voltage-gated $K^+$ channels which contribute to AP repolarization, both of which are downregulated following IoN chronic constriction injury (IoN-CCI) in rats (Kanda et al., 2021; Takeda et al., 2011). The large-conductance $Ca^{2+}$-activated $K^+$ channels (BKCa), which contribute to AP afterhyperpolarization, are also downregulated after IoN-CCI (Liu et al., 2015). In contrast, expression of KCNQ2/3 channels which mediate the M-type outward $K^+$

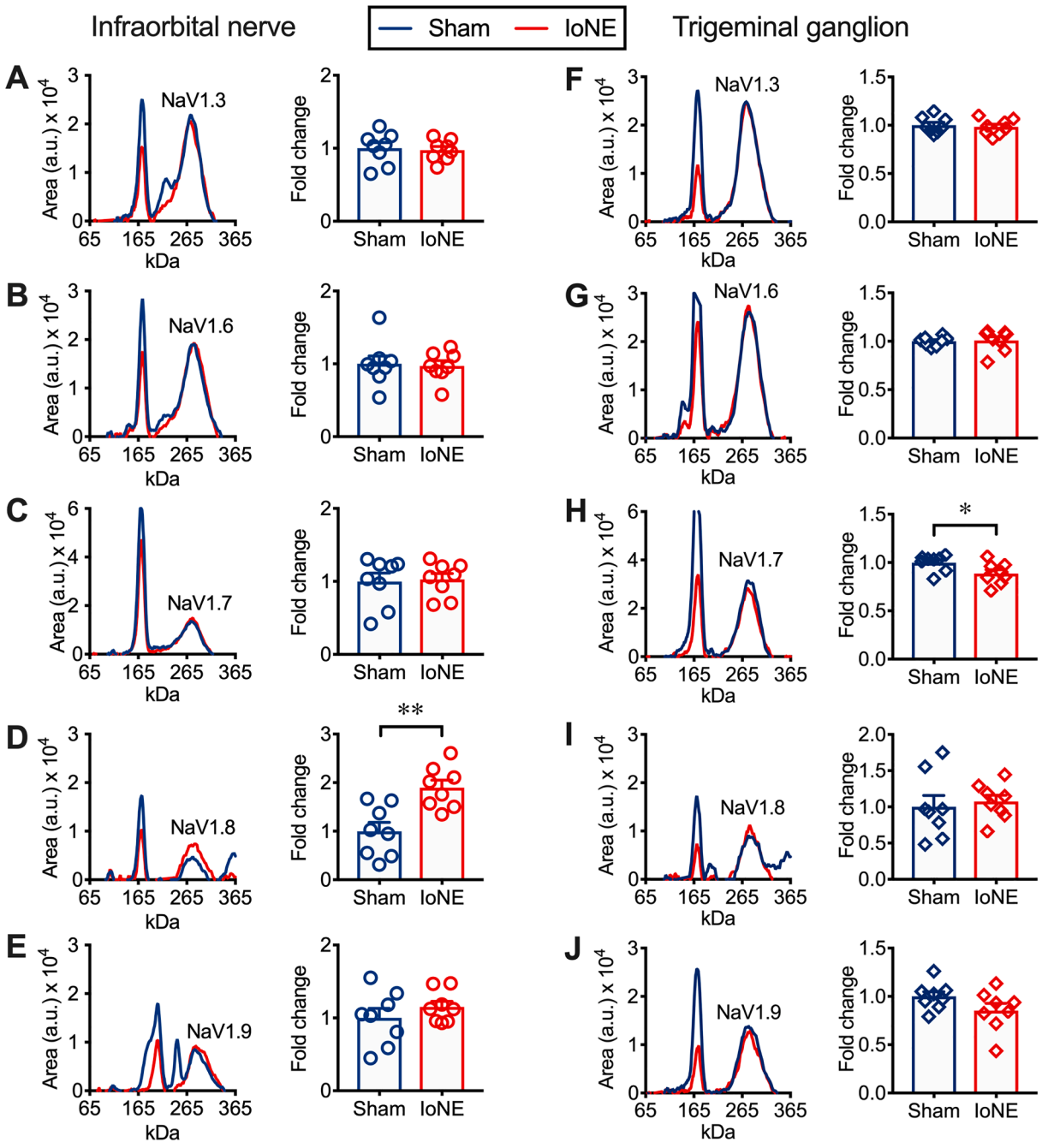


**Fig. 7.** Quantitative protein analysis of the plasma membrane fraction of ipsilateral infraorbital nerve and trigeminal ganglion samples showing voltage gated sodium channel (NaV) subtype expression in Sham and infraorbital nerve entrapment (IoNE) rats measured at ~2 weeks post-surgery. A-J. Spectral graphs on left show group averages (n = 8/group) of target peaks: NaV1.3 (A, F); NaV1.6 (B, G); NaV1.7 (C, H); NaV1.8 (D, I); NaV1.9 (E, J). Bar graphs on the right are group averages of target proteins normalized to total protein and to the mean of the Sham group. *, $p < 0.05$; **, $p < 0.01$ Sham vs IoNE, unpaired *t*-test. Note: The plasma membrane expression of NaV1.8 is significantly increased in the infraorbital nerve of IoNE rats compared to sham rats.

currents is increased after IoN-CCI, suggesting compensatory attempts to limit injury-induced trigeminal hyperexcitability (Ling et al., 2018; Abd-Elsayed et al., 2015).

We observed that IoNE increased the axonal mRNA levels of NaV1.3, NaV1.7, and NaV1.8 while decreasing the transcript levels of most NaVs in the TG. The current findings on the axonal upregulation of NaVs after IoNE to some extent resemble RT-PCR findings from the gingival biopsies of trigeminal neuralgia patients showing upregulation of NaV1.3 and NaV1.7 mRNAs, although the neuronal origin of these transcripts was not investigated (Siqueira et al., 2009). Though the evidence is limited, studies show that NaV1.7 and NaV1.8 expression is also reduced in the spinal dorsal horn after sciatic nerve injury, suggesting that these channels are redistributed mostly to the periphery (Fukuoka et al., 2015; Vysokov et al., 2019). Despite a significant increase in the TTX-sensitivity of A- and C-fiber CAPs after IoNE, our quantitative protein analysis of plasma membrane fraction revealed no significant changes in the expression of NaV1.3 and NaV1.7. In this study, we specifically investigated the expression of NaV proteins in the plasma membrane fraction because it represents a functional expression of cell surface ion channels and receptors. While the amount of mRNA within a cell exemplifies a direct mechanism for regulating protein abundance, there are several instances where a direct correlation between mRNA and

protein levels is not observed (Maier et al., 2009). Protein expression is a highly regulated process exerted by numerous mechanisms, including post-translational modifications that can regulate membrane insertion and function of ion channels and receptors (Curran and Mohler, 2015). In neurons, proteins derived from axonal mRNAs differ from those synthesized in the cell bodies both in their post-translational modification status and cellular functions they exert (Bierhaus et al., 2012; Lee et al., 2021). Although it is not in the scope of the current study to determine the post-translational modification status of NaVs, we expect that the increased TTX sensitivity mainly resulted from a gain of function of TTX-sensitive NaVs derived from axonal mRNAs presumably via distinct post-translational modifications.

Localized mRNA translation has a fundamental role in neuronal development, maintenance, and repair and is key to nociceptor plasticity that drives persistent pain symptoms in many chronic pain states (Kandasamy and Price, 2015; Khoutorsky and Price, 2018; Lackovic et al., 2021; Yousuf et al., 2021). We have shown previously that neuropathy-induced axonal mRNAs differ from those restricted to neuronal soma in their 3′ untranslated regions (UTRs). In the case of NaV1.8 mRNA, the alternative cleavage and polyadenylation of its 3′ UTR region promote peripheral axonal trafficking after nerve injury (Hirai et al., 2017). The subcellular localization of mRNAs, stability, and local translation are regulated by RNA binding proteins, including poly (A)-binding proteins necessary for the expression of inflammatory pain (Barragan-Iglesias et al., 2018; Turner-Bridger et al., 2020). Thus, it remains to be investigated if the axonal redistribution of NaV1.3, NaV1.7, and NaV1.8 mRNAs after IoNE is driven by the same RNA-binding proteins. If so, targeting the mechanisms of their axonal redistribution would provide a novel means to reduce abnormal activation of injured trigeminal nerves.

The current study has several limitations that could be addressed in future experiments. One limitation is that we did not explore possible sex differences in the contribution of NaV subtypes to IoNE-induced changes in axonal signal propagation. In addition, we did not investigate changes in behavioral responses to heat and cold stimuli after IoNE. Although current data provides electrophysiology and molecular evidence for the peripheral axonal redistribution of NaV1.3, NaV1.7, and NaV1.8 after IoNE, we did not explore how these changes contribute to IoNE induced pain behaviors. Our interpretation of the electrophysiological data is also limited by the lack of full concentration–response data for the various NaV blockers used. Another limitation is that while our qPCR data shows axonal upregulation of NaV1.3, NaV1.7, and NaV1.8 mRNAs, the relative expression levels of these NaVs in Aβ-, Aδ-, and C-fiber types remains to be investigated. In addition, while we are aware of the preferential localization of some NaVs in distal axons (Akin et al., 2019; Klein et al., 2017), we did not localize changes in expression of NaVs along the entire length of the affected TG neurons. Some of these limitations could be addressed with molecular imaging and retrograde labeling approaches. Overall, our data suggest that increased axonal expression of NaV1.8 and enhanced sensitivity to axonal conduction block by A-803467 after IoNE contributes to increased axonal signal propagation after infraorbital nerve injury. Our data also highlight the involvement of select TTX-sensitive NaVs in IoNE-induced increases in axonal signal conduction.

## Funding and disclosure

This work was supported by NIH grants CA196263, AA024527, and the Migraine Research Foundation grant 20190437. The authors declare no competing financial interests.

## CRediT authorship contribution statement

**Yatendra Mulpuri:** Conceptualization, Methodology, Validation, Formal analysis, Investigation, Writing – original draft, Writing – review & editing. **Toru Yamamoto:** Conceptualization, Methodology, Validation, Formal analysis, Investigation, Writing – original draft, Writing – review & editing. **Ichiro Nishimura:** Conceptualization, Writing – review & editing. **Igor Spigelman:** Conceptualization, Methodology, Investigation, Writing – original draft, Writing – review & editing, Supervision, Project administration, Funding acquisition.

## Acknowledgements

We would like to thank Armen Agahi, Ammar Amjad, Karla Rodriguez, Sara Kohandani, Tristan Chester, and Delila Zaghi for their help with the data analysis.

## Appendix A. Supplementary data

Supplementary data to this article can be found online at https://doi.org/10.1016/j.ynpai.2022.100084.

## References

Abd-Elsayed, A.A., Ikeda, R., Jia, Z., Ling, J., Zuo, X., Li, M., Gu, J.G., 2015. KCNQ channels in nociceptive cold-sensing trigeminal ganglion neurons as therapeutic targets for treating orofacial cold hyperalgesia. Mol Pain 11, 45.

Akin, E.J., Higerd, G.P., Mis, M.A., Tanaka, B.S., Adi, T., Liu, S., Dib-Hajj, F.B., Waxman, S.G., Dib-Hajj, S.D., 2019. Building sensory axons: Delivery and distribution of NaV1.7 channels and effects of inflammatory mediators. Sci Adv 5, eaax4755.

Alpsan, D., Lal, S., 1980. Combined light- and electron-microscopic study of the rat saphenous nerve. Acta Anat (Basel) 106 (1), 141–149.

Alsaloum, M., Higerd, G.P., Effraim, P.R., Waxman, S.G., 2020. Status of peripheral sodium channel blockers for non-addictive pain treatment. Nat Rev Neurol 16 (12), 689–705.

Baroni, D., Picco, C., Barbieri, R., Moran, O., 2014. Antisense-mediated post-transcriptional silencing of SCN1B gene modulates sodium channel functional expression. Biol Cell 106 (1), 13–29.

Barragan-Iglesias, P., Lou, T.F., Bhat, V.D., Megat, S., Burton, M.D., Price, T.J., Campbell, Z.T., 2018. Inhibition of Poly(A)-binding protein with a synthetic RNA mimic reduces pain sensitization in mice. Nat Commun 9, 10.

Benoliel, R., Kahn, J., Eliav, E., 2012. Peripheral painful traumatic trigeminal neuropathies. Oral Dis 18 (4), 317–332.

Benoliel, R., Heir, M., Eliav, G., 2008. Neuropathic orofacial pain. In: Sharav, Y., Benoliel, R. (Eds.), Orofacial Pain and Headache. Mosby, Edinburgh, pp. 255–294.

Bierhaus, A., Fleming, T., Stoyanov, S., Leffler, A., Babes, A., Neacsu, C., Sauer, S.K., Eberhardt, M., Schnölzer, M., Lasitschka, F., Neuhuber, W.L., Kichko, T.I., Konrade, I., Elvert, R., Mier, W., Pirags, V., Lukic, I.K., Morcos, M., Dehmer, T., Rabbani, N., Thornalley, P.J., Edelstein, D., Nau, C., Forbes, J., Humpert, P.M., Schwaninger, M., Ziegler, D., Stern, D.M., Cooper, M.E., Haberkorn, U., Brownlee, M., Reeh, P.W., Nawroth, P.P., 2012. Methylglyoxal modification of Nav1.8 facilitates nociceptive neuron firing and causes hyperalgesia in diabetic neuropathy. Nat Med 18 (6), 926–933.

Bird, E.V., Christmas, C.R., Loescher, A.R., Smith, K.G., Robinson, P.P., Black, J.A., Waxman, S.G., Boissonade, F.M., 2013. Correlation of Nav1.8 and Nav1.9 sodium channel expression with neuropathic pain in human subjects with lingual nerve neuromas. Mol Pain 9, 52.

Black, J.A., Frezel, N., Dib-Hajj, S.D., Waxman, S.G., 2012. Expression of Nav1.7 in DRG neurons extends from peripheral terminals in the skin to central preterminal branches and terminals in the dorsal horn. Mol Pain 8, 82.

Bozik, M.E., Mather, J.L., Kramer, W.G., Gribkoff, V.K., Ingersoll, E.W., 2011. Safety, tolerability, and pharmacokinetics of KNS-760704 (dexpramipexole) in healthy adult subjects. J Clin Pharmacol 51, 1177–1185.

Chew, L.A., Bellampalli, S.S., Dustrude, E.T., Khanna, R., 2019. Mining the Nav1.7 interactome: Opportunities for chronic pain therapeutics. Biochem Pharmacol 163, 9–20.

Curran, J., Mohler, P.J., 2015. Alternative paradigms for ion channelopathies: disorders of ion channel membrane trafficking and posttranslational modification. Annu Rev Physiol 77 (1), 505–524.

Daou, I., Beaudry, H., Ase, A.R., Wieskopf, J.S., Ribeiro-da-Silva, A., Mogil, J.S., Seguela, P., 2016. Optogenetic Silencing of Nav1.8-Positive Afferents Alleviates Inflammatory and Neuropathic Pain. eNeuro 3.

DaSilva, A.F., DosSantos, M.F., 2012. The role of sensory fiber demography in trigeminal and postherpetic neuralgias. J Dent Res 91 (1), 17–24.

Djouhri, L., Lawson, S.N., 2004. Abeta-fiber nociceptive primary afferent neurons: a review of incidence and properties in relation to other afferent A-fiber neurons in mammals. Brain Res Brain Res Rev 46, 131–145.

Fukuoka, T., Miyoshi, K., Noguchi, K., 2015. De novo expression of Nav1.7 in injured putative proprioceptive afferents: Multiple tetrodotoxin-sensitive sodium channels are retained in the rat dorsal root after spinal nerve ligation. Neuroscience 284, 693–706.

Gasser, H.S., Grundfest, H., 1939. Axon diameters in relation to the spike dimensions and the conduction velocity in mammalian A fibers. Am. J. Physiol. 127 (2), 393–414.

Gold, M.S., Weinreich, D., Kim, C.-S., Wang, R., Treanor, J., Porreca, F., Lai, J., 2003. Redistribution of Na(V)1.8 in uninjured axons enables neuropathic pain. J Neurosci 23 (1), 158–166.
Goodwin, G., McMurray, S., Stevens, E.B., Denk, F., McMahon, S.B., 2021. Examination of the contribution of Nav1.7 to axonal propagation in nociceptors. Pain.
Hargreaves, K.M., 2011. Orofacial pain. Pain 152, S25–S32.
Harper, A.A., Lawson, S.N., 1985. Conduction velocity is related to morphological cell type in rat dorsal root ganglion neurones. J Physiol 359, 31–46.
Hirai, T., Mulpuri, Y., Cheng, Y., Xia, Z., Li, W., Ruangsri, S., Spigelman, I., Nishimura, I., 2017. Aberrant plasticity of peripheral sensory axons in a painful neuropathy. Sci Rep 7, 3407.
Hoffmann, T., Sharon, O., Wittmann, J., Carr, R.W., Vyshnevska, A., Col, R.D., Nassar, M. A., Reeh, P.W., Weidner, C., 2018. NaV1.7 and pain: contribution of peripheral nerves. Pain 159 (3), 496–506.
Jurcakova, D., Ru, F., Kollarik, M., Sun, H., Krajewski, J., Undem, B.J., 2018. Voltage-Gated Sodium Channels Regulating Action Potential Generation in Itch-, Nociceptive-, and Low-Threshold Mechanosensitive Cutaneous C-Fibers. Mol Pharmacol 94 (3), 1047–1056.
Kanda, H., Ling, J., Chang, Y.-T., Erol, F., Viatchenko-Karpinski, V., Yamada, A., Noguchi, K., Gu, J.G., 2021. Kv4.3 Channel Dysfunction Contributes to Trigeminal Neuropathic Pain Manifested with Orofacial Cold Hypersensitivity in Rats. J Neurosci 41 (10), 2091–2105.
Kandasamy, R., Price, T.J., 2015. The pharmacology of nociceptor priming. Handb Exp Pharmacol 227, 15–37.
Kernisant, M., Gear, R.W., Jasmin, L., Vit, J.-P., Ohara, P.T., 2008. Chronic constriction injury of the infraorbital nerve in the rat using modified syringe needle. J Neurosci Methods 172 (1), 43–47.
Khoutorsky, A., Price, T.J., 2018. Translational Control Mechanisms in Persistent Pain. Trends Neurosci 41 (2), 100–114.
Kitagawa, J., Takeda, M., Suzuki, I., Kadoi, J., Tsuboi, Y., Honda, K., Matsumoto, S., Nakagawa, H., Tanabe, A., Iwata, K., 2006. Mechanisms involved in modulation of trigeminal primary afferent activity in rats with peripheral mononeuropathy. Eur J Neurosci 24 (7), 1976–1986.
Klein, A.H., Vyshnevska, A., Hartke, T.V., De Col, R., Mankowski, J.L., Turnquist, B., Bosmans, F., Reeh, P.W., Schmelz, M., Carr, R.W., Ringkamp, M., 2017. Sodium Channel Nav1.8 Underlies TTX-Resistant Axonal Action Potential Conduction in Somatosensory C-Fibers of Distal Cutaneous Nerves. J Neurosci 37 (20), 5204–5214.
Koh, W., Lim, H., Chen, X., 2021. Atypical triggers in trigeminal neuralgia: the role of A-delta sensory afferents in food and weather triggers. Korean J Pain 34 (1), 66–71.
Lackovic, J., Price, T.J., Dussor, G., 2021. De novo protein synthesis is necessary for priming in preclinical models of migraine. Cephalalgia 41 (2), 237–246.
Lai, J., Porreca, F., Hunter, J.C., Gold, M.S., 2004. Voltage-gated sodium channels and hyperalgesia. Annu Rev Pharmacol Toxicol 44 (1), 371–397.
Lee, S.J., Zdradzinski, M.D., Sahoo, P.K., Kar, A.N., Patel, P., Kawaguchi, R., Aguilar, B. J., Lantz, K.D., McCain, C.R., Coppola, G., Lu, Q., Twiss, J.L., 2021. Selective axonal translation of the mRNA isoform encoding prenylated Cdc42 supports axon growth. J Cell Sci 134.
Ling, J., Erol, F., Gu, J.G., 2018. Role of KCNQ2 channels in orofacial cold sensitivity: KCNQ2 upregulation in trigeminal ganglion neurons after infraorbital nerve chronic constrictive injury. Neurosci Lett 664, 84–90.
Liu, C.-Y., Lu, Z.-Y., Li, N.a., Yu, L.-H., Zhao, Y.-F., Ma, B., 2015. The role of large-conductance, calcium-activated potassium channels in a rat model of trigeminal neuropathic pain. Cephalalgia 35 (1), 16–35.
Liu, M.-X., Zhong, J., Xia, L., Dou, N.-N., Li, S.-T., 2020. IL-6 contributes to Nav1.3 up-regulation in trigeminal nerve following chronic constriction injury. Neurol Res 42 (6), 504–514.
Maier, T., Guell, M., Serrano, L., 2009. Correlation of mRNA and protein in complex biological samples. FEBS Lett 583, 3966–3973.
McCormack, K., Santos, S., Chapman, M.L., Krafte, D.S., Marron, B.E., West, C.W., Krambis, M.J., Antonio, B.M., Zellmer, S.G., Printzenhoff, D., Padilla, K.M., Lin, Z., Wagoner, P.K., Swain, N.A., Stupple, P.A., de Groot, M., Butt, R.P., Castle, N.A., 2013. Voltage sensor interaction site for selective small molecule inhibitors of voltage-gated sodium channels. Proc Natl Acad Sci U S A 110 (29), E2724–E2732.
Minett, M.S., Nassar, M.A., Clark, A.K., Passmore, G., Dickenson, A.H., Wang, F., Malcangio, M., Wood, J.N., 2012. Distinct Nav1.7-dependent pain sensations require different sets of sensory and sympathetic neurons. Nat Commun 3, 791.
Mosconi, T., Kruger, L., 1996. Fixed-diameter polyethylene cuffs applied to the rat sciatic nerve induce a painful neuropathy: ultrastructural morphometric analysis of axonal alterations. Pain 64, 37–57.
Novakovic, S.D., Tzoumaka, E., McGivern, J.G., Haraguchi, M., Sangameswaran, L., Gogas, K.R., Eglen, R.M., Hunter, J.C., 1998. Distribution of the tetrodotoxin-resistant sodium channel PN3 in rat sensory neurons in normal and neuropathic conditions. J Neurosci 18 (6), 2174–2187.
Pineda-Farias, J.B., Loeza-Alcocer, E., Nagarajan, V., Gold, M.S., Sekula, R.F., 2021. Mechanisms underlying the selective therapeutic efficacy of carbamazepine for attenuation of trigeminal nerve injury pain. J Neurosci 41 (43), 8991–9007.
Reinhold, A.K., Schwabe, J., Lux, T.J., Salvador, E., Rittner, H.L., 2018. Quantitative and Microstructural Changes of the Blood-Nerve Barrier in Peripheral Neuropathy. Front Neurosci 12, 936.
Robinson, P.P., Boissonade, F.M., Loescher, A.R., Smith, K.G., Yates, J.M., Elcock, C., Bird, E.V., Davies, S.L., Smith, P.L., Vora, A.R., 2004. Peripheral mechanisms for the initiation of pain following trigeminal nerve injury. Journal of Orofacial Pain 18, 287–292.
Rosker, C., Lohberger, B., Hofer, D., Steinecker, B., Quasthoff, S., Schreibmayer, W., 2007. The TTX metabolite 4,9-anhydro-TTX is a highly specific blocker of the Na (v1.6) voltage-dependent sodium channel. Am J Physiol Cell Physiol 293 (2), C783–C789.
Roza, C., Laird, J.M.A., Souslova, V., Wood, J.N., Cervero, F., 2003. The tetrodotoxin-resistant Na+ channel Nav1.8 is essential for the expression of spontaneous activity in damaged sensory axons of mice. J Physiol 550 (3), 921–926.
Ruangsri, S., Lin, A., Mulpuri, Y., Lee, K., Spigelman, I., Nishimura, I., 2011. Relationship of axonal voltage-gated sodium channel 1.8 (NaV1.8) mRNA accumulation to sciatic nerve injury-induced painful neuropathy in rats. J Biol Chem 286 (46), 39836–39847.
Salvatierra, J., Diaz-Bustamante, M., Meixiong, J., Tierney, E., Dong, X., Bosmans, F., 2018. A disease mutation reveals a role for NaV1.9 in acute itch. J Clin Invest 128 (12), 5434–5447.
Samad, O.A., Tan, A.M., Cheng, X., Foster, E., Dib-Hajj, S.D., Waxman, S.G., 2013. Virus-mediated shRNA knockdown of Na(v)1.3 in rat dorsal root ganglion attenuates nerve injury-induced neuropathic pain. Mol Ther 21 (1), 49–56.
Shinoda, M., Imamura, Y., Hayashi, Y., Noma, N., Okada-Ogawa, A., Hitomi, S., Iwata, K., 2021. Orofacial Neuropathic Pain-Basic Research and Their Clinical Relevancies. Front Mol Neurosci 14, 691396.
Siqueira, S.R.D.T., Alves, B., Malpartida, H.M.G., Teixeira, M.J., Siqueira, J.T.T., 2009. Abnormal expression of voltage-gated sodium channels Nav1.7, Nav1.3 and Nav1.8 in trigeminal neuralgia. Neuroscience 164 (2), 573–577.
Smith, E.S., Purfürst, B., Grigoryan, T., Park, T.J., Bennett, N.C., Lewin, G.R., 2012. Specific paucity of unmyelinated C-fibers in cutaneous peripheral nerves of the African naked-mole rat: comparative analysis using six species of Bathyergidae. J Comp Neurol 520 (12), 2785–2803.
Sugimoto, T., Takemura, M., Sakai, A., Ishimaru, M., 1986. Cell size analysis of trigeminal primary afferent neurons comprizing individual peripheral branches of the rat mandibular nerve. Exp Neurol 93 (3), 565–573.
Sugimoto, T., Takemura, M., Wakisaka, S., 1988. Cell size analysis of primary neurons innervating the cornea and tooth pulp of the rat. Pain 32, 375–381.
Sun, J., Li, N., Duan, G., Liu, Y., Guo, S., Wang, C., Zhu, C., Zhang, X., 2018. Increased Nav1.7 expression in the dorsal root ganglion contributes to pain hypersensitivity after plantar incision in rats. Mol Pain 14, 1744806918782323.
Takeda, M., Tsuboi, Y., Kitagawa, J., Nakagawa, K., Iwata, K., Matsumoto, S., 2011. Potassium channels as a potential therapeutic target for trigeminal neuropathic and inflammatory pain. Mol Pain 7, 5.
Thakor, D.K., Lin, A., Matsuka, Y., Meyer, E.M., Ruangsri, S., Nishimura, I., Spigelman, I., 2009. Increased peripheral nerve excitability and local NaV1.8 mRNA up-regulation in painful neuropathy. Mol Pain 5, 14.
Turner-Bridger, B., Caterino, C., Cioni, J.-M., 2020. Molecular mechanisms behind mRNA localization in axons. Open Biology 10 (9), 200177.
Urru, M., Muzzi, M., Coppi, E., Ranieri, G., Buonvicino, D., Camaioni, E., Coppini, R., Pugliese, A.M., Tanaka, B., Estacion, M., Waxman, S.G., Dib-Hajj, S.D., Chiarugi, A., 2020. Dexpramipexole blocks Nav1.8 sodium channels and provides analgesia in multiple nociceptive and neuropathic pain models. Pain 161 (4), 831–841.
Villiere, V., McLachlan, E.M., 1996. Electrophysiological properties of neurons in intact rat dorsal root ganglia classified by conduction velocity and action potential duration. J Neurophysiol 76 (3), 1924–1941.
Vysokov, N., McMahon, S.B., Raouf, R., 2019. The role of NaV channels in synaptic transmission after axotomy in a microfluidic culture platform. Sci Rep 9, 12915.
Waxman, S.G., Cummins, T.R., Dib-Hajj, S., Fjell, J., Black, J.A., 1999. Sodium channels, excitability of primary sensory neurons, and the molecular basis of pain. Muscle Nerve 22 (9), 1177–1187.
Waxman, S.G., Kocsis, J.D., Black, J.A., 1994. Type III sodium channel mRNA is expressed in embryonic but not adult spinal sensory neurons, and is reexpressed following axotomy. J Neurophysiol 72 (1), 466–470.
Waxman, S.G., Zamponi, G.W., 2014. Regulating excitability of peripheral afferents: emerging ion channel targets. Nat Neurosci 17 (2), 153–163.
Xie, M.-X., Zhang, X.-L., Xu, J., Zeng, W.-A., Li, D., Xu, T., Pang, R.-P., Ma, K.e., Liu, X.-G., 2019. Nuclear Factor-kappaB Gates Nav1.7 Channels in DRG Neurons via Protein-Protein. Interaction. 19, 623–633.
Yousuf, M.S., Shiers, S.I., Sahn, J.J., Price, T.J., Dantzer, R., 2021. Pharmacological Manipulation of Translation as a Therapeutic Target for Chronic Pain. Pharmacol Rev 73 (1), 59–88.
Zotova, E.G., Arezzo, J.C., 2013. Non-invasive evaluation of nerve conduction in small diameter fibers in the rat. Physiology journal 2013, 1–11.